(1990); H. Talon, L. Fleury, J. Bernard, M. Orrit, *J. Opt. Soc. Am. B* **9**, 825 (1992).

6. K. H. Drexhage, *J. Lumin.* **12**, 693 (1970).
7. W. Lukosz and R. E. Kunz, *J. Opt. Soc. Am.* **67**, 1607 (1977); *ibid.*, p. 1615; W. Lukosz, *ibid.* **69**, 1495 (1979).
8. T. P. Burghardt and N. L. Thompson, *Biophys. J.* **46**, 729 (1984); N. L. Thompson, H. M. McConnell, T. P. Burghardt, *ibid.*, p. 739.
9. E. H. Hellen and D. Axelrod, *J. Opt. Soc. Am. B* **4**, 337 (1987).
10. T. Hirshfeld, *Appl. Opt.* **15**, 2965 (1976).
11. D. C. Nguyen, R. A. Keller, J. H. Jett, J. C. Martin, *Anal. Chem.* **59**, 2158 (1987).
12. K. Peck, L. Stryer, A. N. Glazer, R. A. Mathies, *Proc. Natl. Acad. Sci. U.S.A.* **86**, 4087 (1989).
13. E. Betzig and J. K. Trautman, *Science* **257**, 189 (1992).
14. ———, T. D. Harris, J. S. Weiner, R. L. Kostelak, *ibid.* **251**, 1468 (1991).
15. The entire optical path for these experiments was as follows: (i) laser light source (green He-Ne, λ = 543.5 nm for random polarization and emission polarization images, Kr^+, λ = 530.9 nm for excitation polarization); (ii) rotatable $\lambda/2$ plate; (iii) rotatable $\lambda/4$ plate (for manipulation of excitation polarization at the aperture); (iv) λ = 535 nm, $\Delta\lambda$ = 35-nm bandpass filter (Omega Optical #535DF35, for rejection of spontaneous emission noise from laser); (v) coupling objective into fiber (Newport Corp. 10×, 0.25 NA); (vi) single mode fiber (~1 m, 3M Corp. #FS-VS-2211) with 100-nm aperture at tapered, Al coated distal end; (vii) sample (see text); (viii) immersion oil (n = 1.518, Zeiss type 518C); (ix) 100×, 1.25 NA objective (Zeiss #44 02 80); (x) Schott glass λ = 570-nm-long pass filter (for rejection of excitation light); (xi) dichroic sheet polarizer (Melles Griot #03 FPG 001, for emission polarization images only); (xii) 160-mm-focal length tube lens of Zeiss Axioskop; (xiii) λ = 633-nm-holographic notch plus filter (Kaiser Optical #HNPF-633-1.0, for rejection of light associated with shear force feedback detection); (xiv) λ = 600 nm, $\Delta\lambda$ = 40-nm bandpass filter (Corion #S40-600, for further rejection of excitation and shear force wavelengths); and (xv) photon counting APD (EG&G #SPCM-200-PQ).
16. U. Dürig, D. W. Pohl, F. Rohner, *J. Appl. Phys.* **59**, 3318 (1986).
17. The potential of near-field fluorescence microscopy has been recognized for some time, with fluorescence detection through subwavelength apertures first reported in E. Betzig, A. Lewis, A. Harootunian, M. Isaacson, and E. Kratschmer [*Biophys. J.* **49**, 269 (1986)], and U. Ch. Fischer [*J. Opt. Soc. Am.* **B3**, 1239 (1986)]. An application demonstrating the current capabilities of fluorescence NSOM as applied to cell biology (in particular, cytoskeletal imaging) can be found in E. Betzig, R. J. Chichester, F. Lanni, and D. L. Taylor [*Bioimaging*, in press].
18. Five microliters of a 2.5 nM solution of dilC$_{12}$(3) was spread over the 18 × 18 mm area of the cover slip to result in the areal density quoted.
19. D. Axelrod, *Biophys. J.* **26**, 557 (1979).
20. Each 2.3 × 2.7 μm image in Fig. 1 was extracted from a 256 × 256 pixel image covering 4 × 4 μm taken with a pixel integration time of 10 ms.
21. The equivalent excitation power extrapolated back to the aperture corresponds to ~3 × 10^{10} counts s^{-1} at the APD. With an extinction coefficient ε ~ 1.5 × 10^5 M^{-1} cm^{-1} for dilC$_{12}$(3), an assumed quantum yield of 0.2, and an estimated collection efficiency (including filters) of 0.2, we then expect ~5 × 10^3 counts s^{-1} per molecule. Although this is almost an order of magnitude less than the peak signal actually measured, the discrepency is understandable in view of the uncertainties in the above numbers, the fact that the molecular interaction with the aperture field is more complicated than this calculation would suggest (that is, Figs. 2 and 3), and the likelihood that evanescent fields contribute significantly to the signal (*16*).
22. With an optimum count rate of ~4 × 10^4 s^{-1} from a single molecule, the Poisson distributed shot noise is $(4 \times 10^4)^{1/2} = 2 \times 10^2$ in a 1 Hz bandwidth. This is 1/200 of the molecular signal. Thus, for other bandwidths we more generally specify the resultant shot noise limited sensitivity as ~0.005 molecules/(Hz)$^{1/2}$. This sensitivity was achieved with 0.4 mW of excitation power at λ = 543.5 nm coupled into the cleaved proximal end of the single mode fiber. Higher sensitivity might be achieved at higher power, with the eventual limit being determined by tip heating effects. Alternatively, the sensitivity could be enhanced by increasing the aperture size beyond 100 nm, but with a concomitant loss of spatial resolution and an eventual limit occurring when the background level (which would also increase due to the increasing effective excitation volume) becomes comparable to the shot noise for the measurement bandwidth chosen.
23. Figure 1F is actually the tenth image of the series, since two images each were taken of Fig. 1, B, C, E, and F.
24. E. Betzig, J. K. Trautman, J. S. Weiner, T. D. Harris, R. Wolfe, *Appl. Opt.* **31**, 4563 (1992).
25. H. A. Bethe, *Phys. Rev.* **66**, 163 (1944).
26. C. J. Bouwkamp, *Philips Res. Rep.* **5**, 321 (1950); *ibid.*, p. 401.
27. E. Betzig, P. L. Finn, J. S. Weiner, *Appl. Phys. Lett.* **60**, 2484 (1992).
28. J. K. Trautman *et al.*, *J. Appl. Phys.* **71**, 4659 (1992); E. Betzig *et al.*, *Appl. Phys. Lett.* **61**, 142 (1992).
29. T. F. Heinz, H. W. K. Tom, Y. R. Shen, *Phys. Rev. A* **28**, 1883 (1983).

30. We thank the following people for their valuable suggestions: R. D. Grober, H. F. Hess, T. D. Harris, J. K. Trautman (AT&T Bell Labs); J. Hwang and M. Edidin (Johns Hopkins University); and F. Lanni (Carnegie Mellon University).

15 September 1993; accepted 19 October 1993

Photon Emission at Molecular Resolution Induced by a Scanning Tunneling Microscope

R. Berndt, R. Gaisch, J. K. Gimzewski, B. Reihl, R. R. Schlittler, W. D. Schneider, M. Tschudy

The tip-surface region of a scanning tunneling microscope (STM) emits light when the energy of the tunneling electrons is sufficient to excite luminescent processes. These processes provide access to dynamic aspects of the local electronic structure that are not directly amenable to conventional STM experiments. From monolayer films of carbon-60 fullerenes on gold(110) surfaces, intense emission is observed when the STM tip is placed above an individual molecule. The diameter of this emission spot associated with carbon-60 is approximately 4 angstroms. These results demonstrate the highest spatial resolution of light emission to date with a scanning probe technique.

A diversity of problems concerning the structure, growth, and aspects of the electronic structure of surfaces and interfaces has been addressed with the use of the STM (*1*). An exciting prospect is to perform local experimentation with individual adsorbed molecules (*2*). Inelastic processes excited by tunneling electrons, which are known to carry specific information on molecular systems (*3*), are difficult to observe by conventional STM. They may, however, be investigated by the detection of photons emitted from the tip-sample region (*4*, *5*). The use of STM as an excitation source that is confined to subnanometer dimensions may open an avenue to combine powerful optical techniques with the high spatial resolution of the STM. Here we report spatially resolved photon emission from individual C_{60} molecules. For hexagonal arrays of C_{60}, we observe the strongest fluorescence when the tip of an STM is centered above an individual molecule. The mapping of this photon signal shows this emission spot to have a lateral extent of about 4 Å.

The experiments were conducted with a custom-built, low-temperature, ultra-high vacuum (UHV) STM operating at a pressure of 10^{-11} mbar and employing temperatures of 5 and 50 K (*6*). Low temperatures improve the stability of imaging at elevated currents and voltages. The samples were prepared in situ by UHV sublimation of C_{60} onto clean, Au(110) 1 × 2–reconstructed surfaces, followed by annealing to 650 K before cooling. The structural properties of thin layers of C_{60} have been thoroughly investigated by STM (*7*). Electrochemically etched W, and Pt, tips were cleaned in the UHV by heating and Ne ion bombardment. Photons were collected with a low *f*-number lens mounted in the cryostat and counted by a cooled photomultiplier. Measurement of the photon signal was performed quasi-simultaneously with the acquisition of constant-current topographs for each image pixel.

A molecularly resolved STM image from a C_{60} monolayer recorded at a constant current of 4.4 nA and a tip voltage V_t of −2.8 V is shown in Fig. 1A. Similar results were obtained for reverse bias (V_t = +2.8 V). The image shows an approximately

R. Berndt, R. Gaisch, W. D. Schneider, Institut de Physique Expérimentale, Université de Lausanne, CH-1015 Lausanne, Switzerland.
J. K. Gimzewski, B. Reihl, R. R. Schlittler, M. Tschudy, IBM Research Division, Zurich Research Laboratory, CH-8803 Rüschlikon, Switzerland.

hexagonal arrangement of the C_{60} molecules with a corrugation amplitude of approximately 1 Å. Particular molecules appear slightly elevated, most likely owing to the large corrugation and steps of the underlying Au(110) surface.

In comparison, the simultaneously recorded photon map (Fig. 1B) is directly correlated with the molecular positions. The detected photon intensity is greatest when the tip acting as a local electron source is placed above an individual C_{60} molecule. The spatial extent of these emission features (full width at half maximum ~4 Å) is smaller than that of the corresponding topographic features. Cross-sectional profiles of topography and photon intensity illustrate this observation quantitatively (Fig. 2, A and B). A few molecules do not exhibit corresponding photon emission maxima, whereas the vast majority give rise to enhanced emission.

From simultaneous measurements of the variation of the tunneling current from the preset value at each image pixel, we can exclude the possibility that the observed contrasts in photon emission are due to fluctuations of the injected current. As to the energy of the observed photons, the low-energy cutoff of the detector and the energy of the incident electrons limit the possible range to 1.5 eV < $h\nu$ < 2.8 eV, where h is Planck's constant and ν is the frequency of a photon.

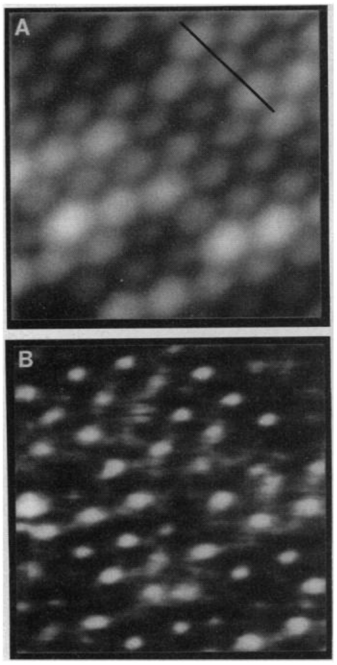

Fig. 1. Gold(110) surface covered with an annealed monolayer of C_{60}. (**A**) Topograph and (**B**) photon map are represented as gray-scale images. Area = 65 Å by 65 Å, tip voltage V_t = − 2.8 V, tunneling current I_t = 4.4 nA, height scale in (A) = 2.5 Å, intensity scale = 800 counts per second, temperature of tip and sample = 50 K.

In the present experiment, the STM tip is used as a source to inject locally a constant current of electrons. Because inelastic tunneling channels contribute only a small fraction to the total tunneling current, which is kept constant, the inelastic contributions are free to fluctuate.

The close proximity of the tip to a metal sample induces localized plasmon modes, which are characterized by a strong electric field in the cavity formed by the tip and the sample (*5, 8*). This sort of resonance mechanism gives rise to photon emission through inelastic tunneling processes from metal surfaces in the STM. These localized modes are similar to those invoked in the classical explanation of surface-enhanced Raman scattering (SERS) (*9*). A variety of factors including the local dielectric properties, surface geometry, and density of states for inelastic processes affects the probability of inelastic tunneling and photon emission from metal surfaces (*10*).

Comparing clean Au surface areas with C_{60}-covered regions, we find that photon emission is strongly suppressed when tunneling occurs on a C_{60} island. This suppression is expected from previous experiments on clean metal surfaces and from model calculations, which have shown that a less efficient electromagnetic coupling at increased tip-sample distances results in decreased photon emission. The molecular contrast within the C_{60} island in Fig. 1B, however, cannot be understood within this kind of model. In such a model, C_{60} acts only as a passive spacer between the tip and sample, which modulates the vertical tip position and thus affects the strength of coupled modes or the angular distribution of the emission. First, we do not observe any contrast reflecting the underlying Au rows, which we find on clean Au(110). Second, in direct contradiction to a scenario involving C_{60} only as a passive spacer, the emission is less intense from intermolecular regions where the tip is closest to the Au substrate than from molecules. Moreover, the angular distribution of light emission from metals was found to be insensitive to tunneling parameters such as tip-sample separation (*11*).

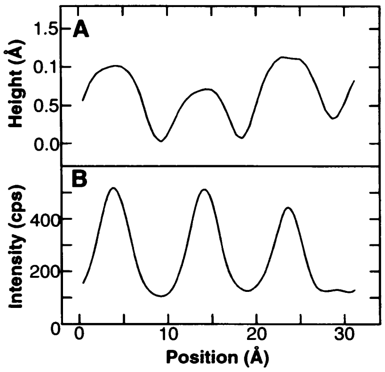

Fig. 2. Cross-sectional profiles of (**A**) topography and (**B**) photon intensity extracted from the section indicated in Fig. 1A. When the STM tip is centered above a C_{60} molecule the emission intensity is maximized regardless of bias polarity.

These findings may indicate that the C_{60} molecules play an active role in the emission process. We suggest that the molecules interact strongly with the electromagnetic modes of the cavity between the tip and the metal sample. Analogous to the case of SERS from molecules in pores of Ag films (*12*), such a confinement effect may dramatically affect the molecular photon emission. Molecular properties possibly involved in the observed emission are excitonic states, as revealed by conventional luminescence studies (*13, 14*), or collective electronic excitations, as have been postulated in the interpretation of electron energy-loss data (*15*). The extreme geometry of the present experiment—the molecules are studied within a nanometer-wide cavity—is expected to modify the emission due to either of these properties in energetic position and width with respect to a conventional fluorescence experiment. The molecular contrast in photon maps and topography is independent of bias polarity (± 2.8 V), which indicates that this contrast does not result from C_{60}-induced changes of the local density of states of the sample. It is, however, consistent with an inelastic tunneling process that involves the molecule.

We have presented a photon emission measurement in which individual molecules packed in nanometer-scale separation are clearly resolved. For the C_{60} molecules studied, the detected photon emission is most intense when the STM tip acting as an excitation source is placed above an individual molecule. In photon emission maps, molecules thus give rise to emission features with an observed diameter of ~4 Å. We tentatively propose that electromagnetic confinement effects may mediate and amplify emission from the coupled system comprising tip, molecule, and substrate. These results suggest that an optical spectroscopic analysis of the emission on the scale of individual molecules can also be achieved. We are now incorporating a highly sensitive optical spectrometer into the system for this purpose (*16*).

REFERENCES AND NOTES

1. H. Rohrer, in *Scanning Tunneling Microscopy and Related Methods*, R. J. Behm, N. Garcia, H. Rohrer, Eds., vol. 184 of NATO Advanced Studies Institutes Series E (Kluwer, Dordrecht, the Netherlands, 1990), p. 1.
2. J. A. Stroscio and D. M. Eigler, *Science* **254**, 1319 (1991).
3. E. L. Wolf, *Principles of Electron Tunneling Spectroscopy* (Oxford Univ. Press, New York, 1985).
4. J. H. Coombs *et al.*, *J. Microsc.* **152**, 325 (1988); J. K. Gimzewski, B. Reihl, J. H. Coombs, R. R. Schlit-

tler, *Z. Phys. B* 72, 497 (1988); J. K. Gimzewski, J. K. Sass, R. R. Schlittler, J. Schott, *Europhys. Lett.* **8**, 435 (1989).
5. R. Berndt, J. K. Gimzewski, P. Johansson, *Phys. Rev. Lett.* **67**, 3796 (1991).
6. R. Gaisch *et al.*, *Ultramicroscopy* **42**, 1621 (1992).
7. T. Hashizume *et al.*, *Jpn. J. Appl. Phys.* **31**, L880 (1992); Y. Z. Li *et al.*, *Science* **252**, 547 (1991); H. P. Lang *et al.*, *Europhys. Lett.* **18**, 29 (1992); J. L. Wragg *et al.*, *Nature* **348**, 623 (1990); R. J. Wilson *et al.*, *ibid.*, p. 621; E. I. Altman and R. J. Colton, *Surf. Sci.* **279**, 49 (1992); T. Chen *et al.*, *Phys. Rev. B* **45**, 14411 (1992); R. Gaisch *et al.*, *Appl. Phys. A* **57**, 207 (1993).
8. B. N. J. Persson and A. Baratoff, *Phys. Rev. Lett.* **68**, 3224 (1992).
9. A. Otto, I. Mrozek, H. Grabhorn, W. Akemann, *J. Phys. Condens. Matter* **4**, 1143 (1992).
10. R. Berndt and J. K. Gimzewski, *Phys. Rev. B* **48**, 4746 (1993).
11. R. Berndt, thesis, University of Basel, Basel, Switzerland (1992).
12. E. V. Albano, S. Daiser, R. Miranda, K. Wandelt, *Surf. Sci.* **150**, 386 (1985).
13. C. Reber *et al.*, *J. Phys. Chem.* **95**, 2127 (1991); M. Matus, H. Kuzmany, E. Sohmen, *Phys. Rev. Lett.* **68**, 2822 (1992).
14. A. T. Werner *et al.*, *Europhys. Conf. Abstr.* **17A**, 1854 (1993).
15. A. Lucas *et al.*, *Phys. Rev. B* **45**, 13694 (1992); M. T. Michalewicz and M. P. Das, *Solid State Commun.* **84**, 1121 (1992).

16. We thank R. L. Whetten for providing the fullerene molecules, W. Andreoni and M. Parrinello for useful discussions, and Ch. Gerber and H. Rohrer for their support. Supported in part by the Swiss National Science Foundation programs NFP24 and NFP24+.

16 August 1993; accepted 26 October 1993

X-ray Linear Dichroism Microscopy

H. Ade* and B. Hsiao

Chemical-specific x-ray linear dichroism was observed in an x-ray microscope as evidenced by changes in relative contrast upon azimuthal rotation of the sample. As a demonstration, thin sections of a partially ordered polymer fiber were examined with a transmission x-ray microscope near the carbon *K*-shell absorption edge to provide chemical-specific imaging at 50-nanometer spatial resolution. The observed dichroism and change in contrast upon rotation arise from the polarization dependence of the near-edge x-ray absorption cross section and can be used to image the orientation of specific chemical bonds.

The structural, morphological, and chemical characterization of multiphase polymers, liquid crystalline polymers, fibers, and composites is critical to our understanding of the mechanical and chemical properties of these materials. A variety of characterization techniques have been used, ranging from electron microscopy to neutron scattering (*1, 2*). None of these techniques can, however, provide information about the orientation of specific chemical bonds in nonisotropic samples at suboptical spatial resolution. We present a technique, x-ray linear dichroism microscopy, that can acquire such information at 50-nm spatial resolution. Another kind of dichroism microscopy, x-ray circular dichroism microscopy, has recently been developed by Stöhr *et al.* (*3*). It provides element-specific magnetization contrast between magnetic domains at a spatial resolution of about 1 μm and addresses a set of applications different from those addressed by the technique presented here.

To demonstrate x-ray linear dichroism microscopy, we used the scanning transmission x-ray microscope (STXM) at the National Synchrotron Light Source (NSLS). Soft x-rays generated by the X1 undulator at NSLS were used, and the microscope's imaging characteristics and performance have been described previously (*4*). We added an azimuthally rotatable sample stage to the microscope (*5*). We also made use of the linear polarization of the undulator output, which is a characteristic of synchrotron radiation so far unexploited in x-ray microscopy. We imaged thin sections of poly(*p*-phenylene terephthalamide) (PPTA) fibers (Kevlar) with a spatial resolution of 50 nm at photon energies that are sensitive to the carbonyl and the aromatic groups of the fiber polymer. Three types of Kevlar fibers were chosen: Kevlar 29, 49, and 149, which differ from each other in the degree of crystallinity (Kevlar 149 is the most and Kevlar 29 is the least crystalline) and the crystalline orientation along the fiber axis (*6*).

We observed x-ray linear dichroism at high spatial resolution in all samples. This is to be expected for a partially oriented and ordered sample such as Kevlar because the near edge x-ray absorption fine structure (NEXAFS) is not only chemically sensitive, but the near edge cross sections strongly depend on the geometric orientation of the chemical bond relative to the electric field vector (*7*). We observed butterfly-like patterns for all of these fibers, consistent with radially symmetric models of the fiber structure. In addition, some thin films of similar Kevlar fibers, prepared separately, exhibited a one-dimensional anisotropy, presumably introduced by the stress during sectioning. These films showed pronounced contrast changes upon rotation and features predominantly oriented perpendicular to the cutting direction.

A small-area spectrum of a Kevlar 49 thin film (0.1 μm thick) cut at 45° relative to the fiber axis as acquired with the STXM is shown in Fig. 1. The most prominent peaks are associated with aromatic (285.5 and 286.3 eV) and carbonyl (288.3 eV) groups. The photon energy can be selectively tuned to these characteristic energies to achieve chemical sensitivity during imaging (*8*); owing to the polarization dependence of NEXAFS, the strong peak at 285.5 eV, for example, would actually disappear if all the aromatic groups were lying in a single plane and the electric field vector of a 100% polarized x-ray beam was also lying in the same plane. The physics of this process is well understood. The intensity observed is proportional to $\cos^2\theta$, where θ is the angle between the electric field vector and the direction of the orbital excited during absorption, which for a π orbital is perpendicular to the aromatic plane (*7*).

The radially symmetric structural model of Kevlar fibers predicts the observation of a butterfly-like pattern in an x-ray linear dichroism image of thin films of the fiber cut at 45° with respect to the fiber axis (*9*). The planes of the two different aromatic groups of the fiber are not the same. They are estimated to be at an angle of 68° with respect to each other (*6*), with the average aromatic ring plane pointing essentially radially outward. Thus, the maximum observable contrast in an image acquired at 285.5 eV is reduced significantly compared with that achievable in a sample having a single aromatic plane. This results in about 15% contrast, which is further reduced by orientational disorder and the

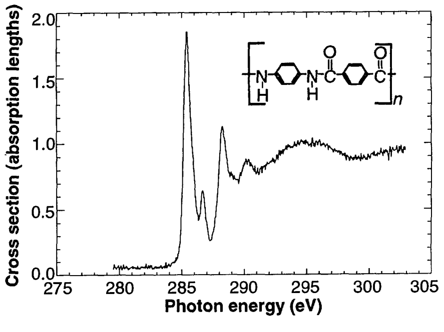

Fig. 1. The NEXAFS spectrum of 0.1 μm² of a 0.1-μm-thick section of Kevlar 49 fiber (inset structure) cut at 45° as acquired with the STXM. The prominent spectral features at 285.5, 286.7, and 288.3 eV are π^* resonances associated with unsaturated bonding in the aromatic and carbonyl groups. The energies are characteristic, providing the means for bond-selective imaging, whereas the intensity depends on polarization and the geometrical orientation of the bonds. The broader feature at 295 eV is a σ^* resonance of the C–C bonds. Total acquisition time was 40 s (*13*).

H. Ade, Department of Physics, North Carolina State University, Raleigh, NC 27695–8202.
B. Hsiao, Experimental Station, DuPont, Wilmington, DE 19880–0302.

---

*To whom correspondence should be addressed.